



HAL
open science

A Modulated Wideband Converter Calibration Technique Based on a Single Measurement of a White Noise Signal with Advanced Resynchronization Preprocessing

Gilles Burel, Anthony Fiche, Roland Gautier, Annaig Martin-Guennou

► **To cite this version:**

Gilles Burel, Anthony Fiche, Roland Gautier, Annaig Martin-Guennou. A Modulated Wideband Converter Calibration Technique Based on a Single Measurement of a White Noise Signal with Advanced Resynchronization Preprocessing. *Electronics*, 2022, 11 (5), pp.774. 10.3390/electronics11050774 . hal-03601692

HAL Id: hal-03601692

<https://hal.science/hal-03601692v1>



Submitted on 11 Jan 2024

HAL is a multi-disciplinary open access archive for the deposit and dissemination of scientific research documents, whether they are published or not. The documents may come from teaching and research institutions in France or abroad, or from public or private research centers.

L'archive ouverte pluridisciplinaire **HAL**, est destinée au dépôt et à la diffusion de documents scientifiques de niveau recherche, publiés ou non, émanant des établissements d'enseignement et de recherche français ou étrangers, des laboratoires publics ou privés.

Article

A Modulated Wideband Converter Calibration Technique Based on a Single Measurement of a White Noise Signal with Advanced Resynchronization Preprocessing

Gilles Burel ^{*}, Anthony Fiche, Roland Gautier  and Annaig Martin-Guennou

Univ Brest, CNRS, Laboratoire des Sciences et Techniques de l'Information, de la Communication et de la Connaissance, CS 93837, 6 avenue Le Gorgeu, CEDEX 3, 29238 Brest, France;

anthony.fiche@univ-brest.fr (A.F.); roland.gautier@univ-brest.fr (R.G.); annaig.guennou@univ-brest.fr (A.M.-G.)

* Correspondence: gilles.burel@univ-brest.fr

Abstract: The Modulated Wideband Converter (MWC) is a blind sub-Nyquist sampling system used especially to monitor wideband spectrum. This system can be realized by existing analog components. From a theoretical point of view, all analog components are assumed ideal. However, this hypothesis is false in practice. Indeed, some imperfections are introduced by analog components such as nonlinearities of mixers, phase/attenuation/selectivity of low-pass filters and desynchronization between modulating waveforms. Consequently, it is necessary to correctly estimate the sensing matrix to ensure correct spectrum reconstruction performance. Conventional calibration methods are based on the measurements of different single tones. However, these approaches need to record several measurements with single-tone inputs. To avoid this problem, this paper presents a new hardware calibration method of MWC by using a single measurement of a white noise signal for radio frequency spectrum monitoring. A preprocessing method is performed to resynchronize input, output and modulating waveforms signals with each other. Our hardware calibration method is applied to our prototype of Compressed Sensing (CS) scheme in order to estimate the corrected sensing matrix. To prove the efficiency of our hardware calibration, reconstruction performances were evaluated with respect to the probability of correct reconstruction and false alarm criteria. These results are compared with those obtained with the theoretical MWC scheme, with our prototype without calibration and with reference calibration.

Keywords: compressed sampling; hardware calibration; modulated wideband converter; signals resynchronization method; spectrum monitoring



Citation: Burel, G.; Fiche, A.; Gautier, R.; Martin-Guennou, A. A Modulated Wideband Converter Calibration Technique Based on a Single Measurement of a White Noise Signal with Advanced Resynchronization Preprocessing. *Electronics* **2022**, *11*, 774. <https://doi.org/10.3390/electronics11050774>

Academic Editor: Massimo Donelli

Received: 31 January 2022

Accepted: 27 February 2022

Published: 2 March 2022

Publisher's Note: MDPI stays neutral with regard to jurisdictional claims in published maps and institutional affiliations.



Copyright: © 2022 by the authors. Licensee MDPI, Basel, Switzerland. This article is an open access article distributed under the terms and conditions of the Creative Commons Attribution (CC BY) license (<https://creativecommons.org/licenses/by/4.0/>).

1. Introduction

Radio frequency spectrum monitoring is a major issue in communications applications due to the expansion of wireless technologies which implies a reduction of available band spectrum. For example, the Internet-of-Things (IoT) communication has recently emerged in many applications such as Smart City which has the advantage of low power consumption. The number of IoT connected devices will explode in the near future. Consequently, a specific bandwidth will be saturated because several wireless devices will be connected at the same time. It is possible to handle this problem by using cognitive radios which are able to manage dynamically the spectrum. During many years, spectrum monitoring has been based on the Shannon–Nyquist sampling theorem [1,2]. Indeed, it is possible to reconstruct a signal by picking samples at periodic time. Mathematically, the Nyquist rate F_{Nyq} is determined for a band-limited spectrum $[F_{min}; F_{max}]$ by $F_e \geq 2 * (F_{max} - F_{min})$ [3]. However, in practice, this method is difficult to use in a wideband context, typically more than 1 GHz. Indeed, Nyquist frequency can exceed the specifications of existing Analog to Digital Converters (ADC) and sampling at a high rate introduces amount of data which requires a huge storage capacity.

Several techniques, depending or not on the knowledge of the carrier frequency, have been developed to monitor a multiband spectrum (random demodulator [4,5], multicorset sampling [6,7], Modulated Wideband Converter [8], quadrature analog-to-information converter [9], time-segmented quadrature analog-to-information converter [10], random triggering based modulated wideband compressive sampling [11] and non uniform wavelet sampling [12,13]). In the case of known carrier frequencies, a band of interest is firstly chosen and the signal is demodulated by its carrier frequency. Unwanted bands of signals were rejected by a low-pass filter. Finally, the selected band is sampled by an ADC at a realistic rate [14]. In the case of unknown carrier frequencies, it is a hard challenge to blindly recover a signal from the measured samples.

One major problem to monitor wideband signal is to choose appropriate ADCs. An ADC is first characterized by a track and hold circuit which tracks the value of the analog input signal and holds it at a constant value between clock cycles. This analog value is then digitized by a quantization module. Therefore, an ADC is generally characterized by an input bandwidth B corresponding to the maximal frequency supported by the Track/Hold module and by a sampling frequency F_s equal to the inverse of the time duration T_s of the quantization processing. Indeed, an ADC can be limited for two main reasons. Firstly, its bandwidth B needs to be equal to the bandwidth of the signal input, which can be huge in practice. Moreover, according to the Shannon–Nyquist sampling theorem, its sampling frequency F_s could be very high, which can not be provided by actual ADCs. The first issue can be addressed by multi channel sampling schemes. Uniform interleaved sampling [15] can be used to sample a wideband signal. Assume that a wideband signal $x(t)$ needs to be sampled at a Nyquist frequency M times higher than the frequency F_s specified by an ADC. Instead of using a single ADC at a high rate, a solution is to use M ADCs in parallel and interleave them with delays. By choosing delays spaced of T_s/M , with $T_s = 1/F_s$, M samples are contained in the periodic time T_s . If samples are multiplexed, the scheme can be seen as a unique ADC with a sampling frequency $F'_s = MF_s$. To respect the Shannon–Nyquist theorem, i.e., $F'_s = MF_s = F_{Nyq}$, it is necessary to fix the ADC sampling frequency $F_s = F_{Nyq}/M$. Consequently, the sampling frequency is reduced by a factor M . Although this approach solves the problem of limitation of the ADC sampling frequency F_s , it still requires an ADC with bandwidth B at least equal to the input signal bandwidth. Moreover, maintaining constant time shifts of the order of T_s/M is difficult to implement [8]. Nonuniform interleaved sampling [16] has also been proposed to sample multiband signals. Compared to the uniform interleaved sampling, delays are irregularly spaced. However, to implement this algorithm, delays are assumed periodic. As in the uniform case, the nonuniform sampling allows the ADC frequency F_s to be reduced by a factor M ; however, it is still also limited because the ADC bandwidth B must be equal to the bandwidth of the input signal. This approach has the advantage of being compressive. However, this method is difficult to use in practice due to the performance of the ADCs.

Recently, a new approach has been proposed allowing sampling at sub-Nyquist rate. This approach is called compressed sensing, or more generally compressive sampling. Compressed sensing has recently emerged as a potential framework for signal acquisition in many applications [17], especially to monitor a wideband spectrum [18]. In [19,20], the authors showed that a finite-dimensional signal which has a sparse representation in some basis can be recovered from a small set of linear measurements. Theoretical aspects of compressed sensing have been largely addressed in the literature. For instance, many studies on the design of the measurements scheme have been proposed as in [21,22]. However, few works have considered practical constraints of compressed sensing. Indeed, the design of the measurements schemes and their application to practical acquisition systems such as spectrum sensing systems remain a central challenge in the field of compressed sensing. More recently, the authors in [8] proposed a new scheme, called Modulated Wideband Converter (MWC), which allows sampling at rates much lower than the Nyquist rate while considering practical implementation issues of compressed sensing. In this work, the band locations are unknown to the user. Generally, the proposed scheme architecture in [8] can

be decomposed into two main steps. Firstly, an analog processing is applied to the input signal in order to create several channels through modulation and filtering. In the second step, each channel is sampled by ADCs.

In this paper, the MWC scheme proposed in [8] is considered which, to the best of our knowledge, seems to be the most convenient scheme in terms of recovering performance, complexity and practical implementation. Some practical implementations of compressed sensing systems have been already proposed [4,23,24]. To realize a prototype of compressed sensing based on MWC scheme, three solutions can be followed. The first solution is to use commercial off-the-shelf components. However, this type of solution had a significant risk in terms of development due to the defects introduced by all components. The second solution would be to develop a custom silicon solution [24]. However, this solution can be very expensive and dicey for testing and debugging steps. The third (chosen solution) solution is to design an analog board with discrete components to achieve this functionality. Some authors have already addressed the design of MWC system and a non-exhaustive list of references is given here [23,25–29]. Our analog board has a number of physical channels M limited to four channels and the length of the modulating sequences L is realistic and set to 96. These parameters will be explained in detail in Section 2.

One important step in compressed sensing framework is the knowledge of the sensing matrix required for the reconstruction step. In the ideal case, the sensing matrix can be perfectly estimated from modulating waveforms. However, in practice, some problems introduced by analog components (such as nonlinearities of mixers, phase/attenuation/selectivity of lowpass filters, desynchronization between modulating waveforms) have been identified by researchers from Technion—Israel Institute of Technology [23]. The authors have proposed a calibration method to estimate the sensing matrix. They estimate one column of the sensing matrix by injecting sine function at a specific frequency. This step is repeated by changing the frequency until all columns of the sensing matrix are estimated. This technique can be considered as a reference. Some researchers have exploited this work to propose calibration algorithms [29–33] based on the measurements of different single tones. In our opinion, one drawback of this procedure is that this task can be time consuming and annoying when the number of columns of the sensing matrix L is high because the same step must be repeated many times. Consequently, the motivation of this paper is to develop a new MWC hardware calibration technique from only one measurement. The idea has been already proposed in [34,35] where the calibration signal is a mixture of single tones.

Table 1 sums up the difference between our MWC calibration method and other MWC calibration methods.

Table 1. Comparison between our MWC calibration method and others MWC calibration methods from the literature.

MWC Calibration Method	Number of Measurements	Calibration Signal	Time Consumption
Israeli et al. [23] Liu et al. [29] Wang et al. [30] Fu et al. [31] Park et al. [32] Alp et al. [33]	$\frac{L}{2} + 1$	single tone	high
Byambadoryj et al. [34]	1	mixture of single tones	low
This paper	1	white noise signal	low

The main contributions of this paper are:

- A prototype of compressed sensing based on MWC scheme has been developed to monitor a wideband spectrum at Nyquist frequency $F_{Nyq} = 1$ GHz. The prototype has $M = 4$ physical channels. The total equivalent sampling rate is equal to $M \times F_s = 291.6$ MHz which is 29.16% of the Nyquist rate.
- The calibration signal is a white noise signal. Compared to methods based on iterative single-tones or mixture of single-tone signals, our new calibration method has the advantage of being more practical in terms of simplicity of implementation and time saving because only one measurement is used to complete the calibration. The calibration signal spectrum is totally flat in the band of interest and covers all the bandwidths of the spectrum to analyze.
- The calibration method uses an advanced resynchronization preprocessing. Our calibration method offers slightly better spectrum reconstruction performances compared to reference method [23].

The remainder of this paper is organized as follows: Section 2 describes the MWC theoretical background. Section 3 presents our prototype of compressed sensing based on MWC scheme. Section 4 presents our calibration method. Section 5 presents spectrum reconstruction performances and examples of spectrum reconstruction obtained with our calibration method from MWC output.

2. MWC Theoretical Background

This section develops the MWC physical scheme and a Nyquist-equivalent model of MWC.

2.1. Physical Scheme

MWC scheme which allows sampling a wideband sparse signal at sub-Nyquist rate has been introduced in [8]. The block diagram of MWC scheme is illustrated in Figure 1. In this scheme, a signal $x(t)$ is modulated by a set of T_p -periodic waveforms $p_i(t)$ on M parallel channels with $i \in [1; M]$. For each channel i , the modulated signal is low-pass filtered with a filter of bandwidth F_s and the filtered signal is sampled at frequency F_s into $y_i[n]$ output samples.

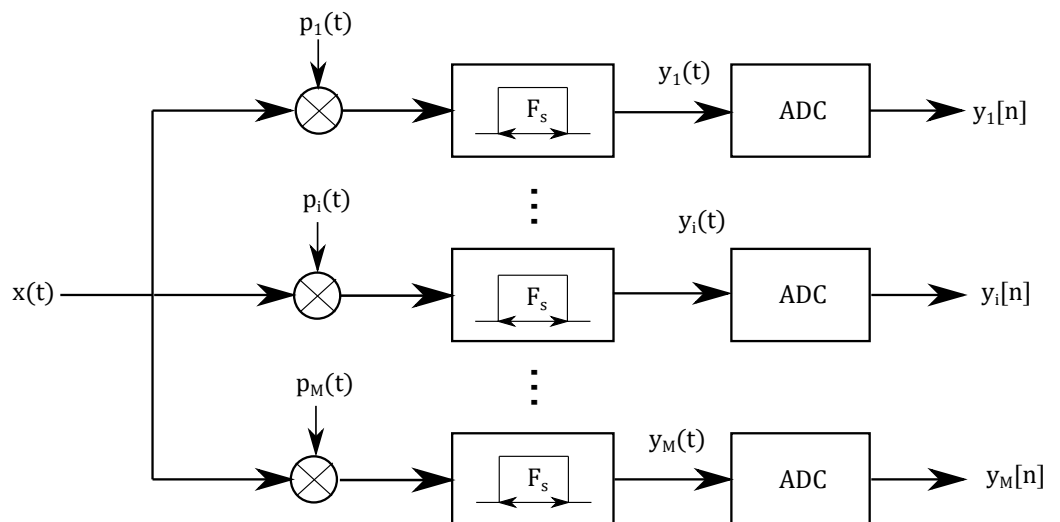


Figure 1. Block diagram of the MWC scheme.

2.2. Nyquist-Equivalent Model of MWC

A Nyquist-equivalent model of MWC, shown in Figure 2, has been introduced in [26]. This MWC-equivalent model modulates the input signal $x(t)$ by carrier frequencies spaced by F_p . Consequently, L channels are processed in parallel and, for each channel, the spectrum $X(f)$ is shifted by a multiple l of the frequency F_p .

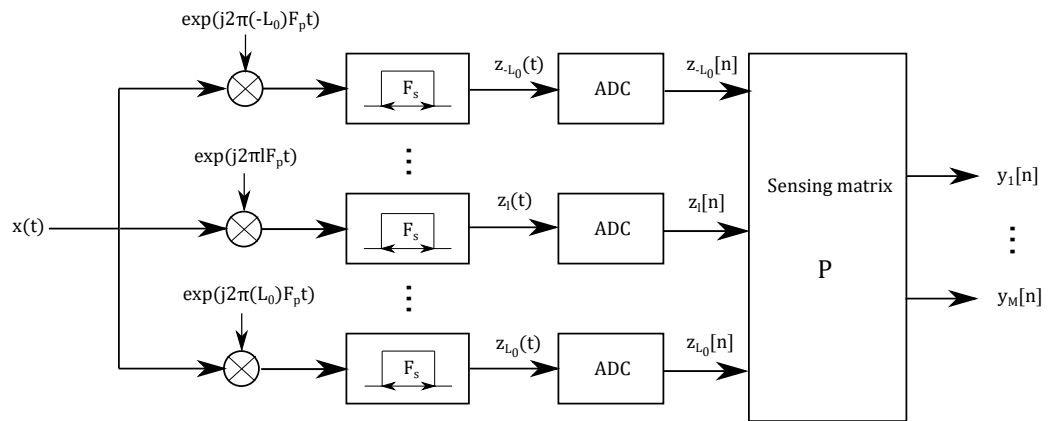


Figure 2. Nyquist-equivalent model of MWC.

Due to the periodic functions, L is determined by computing the ratio between the bandwidth of the input signal and the frequency of periodic functions ($L = \frac{F_{Nyq}}{F_p}$). The L -channels are then low-pass filtered with an ideal filter of bandwidth F_s and response frequency $H(f)$. For each internal channel, low-pass filtered signals are then sampled at frequency F_s into samples $z_l[n]$ with $l \in [-L_0; L_0]$ such that $L_0 = \frac{L-1}{2}$. The output samples $y_i[n]$ are finally obtained by applying a $M \times L$ sensing matrix \mathbf{P} such as:

$$\mathbf{y} = \mathbf{Pz} \tag{1}$$

The system can also be written as:

$$y_i[n] = \sum_{l=-L_0}^{L_0} p_{il}z_l[n] \tag{2}$$

where p_{il} are the Fourier coefficients of the T_p -periodic waveform p_i .

Each internal channel $z_l[n]$ can be computed by:

$$z_l[n] = \text{IDFT}(X(f - lF_p)H(f))(nT_s) \tag{3}$$

where IDFT is the Inverse Discrete Fourier Transform.

In practice, it is impossible to deploy all mixers, low-pass filters and ADCs for all channels when M (number of channels) is high. In [36], the authors introduced a collapsing factor $q = \frac{F_s}{F_p}$ which allows to reduce the number of physical channels by a factor q . Theoretically, the system works as if there are $q \times M$ channels and the output is sampled at F_p . Consequently, the system defined by Equation (1) can be extended to $q \times M$ outputs:

$$\mathbf{y_e} = \mathbf{P_ez} \tag{4}$$

with a $qM \times L$ sensing matrix $\mathbf{P_e}$ which is an extension version of \mathbf{P} . For the rest of the paper, the extended version of matrices are used for the reconstruction.

The challenge is to reconstruct the signal $x(t)$ or only its spectrum depending on the application, with knowledge of \mathbf{y}_e and the matrix \mathbf{P}_e by solving Equation (4). To achieve this task, the authors [8] introduced a Continuous-To-Finite (CTF) reconstruction block. In this paper, the number s of active channels are estimated from \mathbf{y}_e by using different classical algorithms such as Akaike Information Criterion [37] or Minimum Description Length [38]. By knowing \mathbf{y}_e , \mathbf{P}_e and s , the solution $\hat{\mathbf{z}}$ of Equation (4) is estimated by the Orthogonal Matching Pursuit (OMP) algorithm [39].

2.3. Parameters Constraints

Performance of MWC scheme depends on several parameters such as the number of channels M , the sampling frequency F_s , the T_p -periodic sequences $p_i(t)$ and their period T_p . One important problem is how to choose these parameters. To set these parameters, some conditions must be met in order to achieve successful signal recovering: the bandwidth filter F_s and the hypothesis of sparsity of the signal.

The modulation operator shifts the spectrum $X(f)$ of the signal $x(t)$ by frequencies multiple of F_p . Therefore, it is necessary to fix $F_s \geq F_p$ otherwise some frequency bands will not be represented on any channel [8] and, therefore, signal recovering will fail. When considering $F_s = F_p$, the frequency bands on the different channels are disjointed.

For the condition of sparsity, knowing the $qM \times L$ sensing matrix \mathbf{P}_e and the measurements vector \mathbf{y}_e and in order to recover \mathbf{z} , the sensing matrix \mathbf{P}_e needs to be invertible or pseudo-invertible, i.e., $qM \geq L$. Under this condition, we obtained:

$$qMF_s \geq LF_s \geq \frac{F_{Nyq}}{F_p} F_s \geq F_{Nyq} \quad (5)$$

However, Equation (5) shows a contradiction because the sub-Nyquist condition is not verified anymore. Therefore, the hypothesis on the signal sparsity needs to be assumed on the multiband signal $x(t)$ to be able to recover the spectrum. $x(t)$ can be considered sparse in the frequency domain if only some unknown sub-bands of the spectrum $X(f)$ are occupied, represented by the active components in vector \mathbf{z} . By assuming the sparsity of \mathbf{z} (which is a consequence of the sparsity of $x(t)$ in the frequency domain), it is possible with $qM < L$ to recover the vector \mathbf{z} from the measurements vector \mathbf{y}_e .

The next section describes our prototype of compressed sensing based on MWC scheme.

3. MWC Hardware Prototype

The genesis of this work, which is a part of a large innovative project dedicated to coastal surveillance, is to monitor a wideband spectrum at Nyquist frequency $F_{Nyq} = 1$ GHz. To the best of our knowledge, the MWC seems to be the most convenient scheme in terms of recovering performance, complexity and practical implementation. Some prototypes [23,25,28] of compressed sampling scheme based on MWC with different parameters have been already developed. For simplicity of implementation, the number of physical channels M must be realistic as in [23,25,28]. For simplicity of generation, the length of mixing sequences L has been chosen lower than the length of mixing sequences used in [23,25,28]. The values of these parameters are given in Section 3.1. Figure 3 shows our prototype of compressed sampling scheme based on MWC.

In this section, we motivate the choice of the prototype parameters and we present the analog board. An example of spectrum reconstruction without calibration is directly processed from data acquired by the prototype.

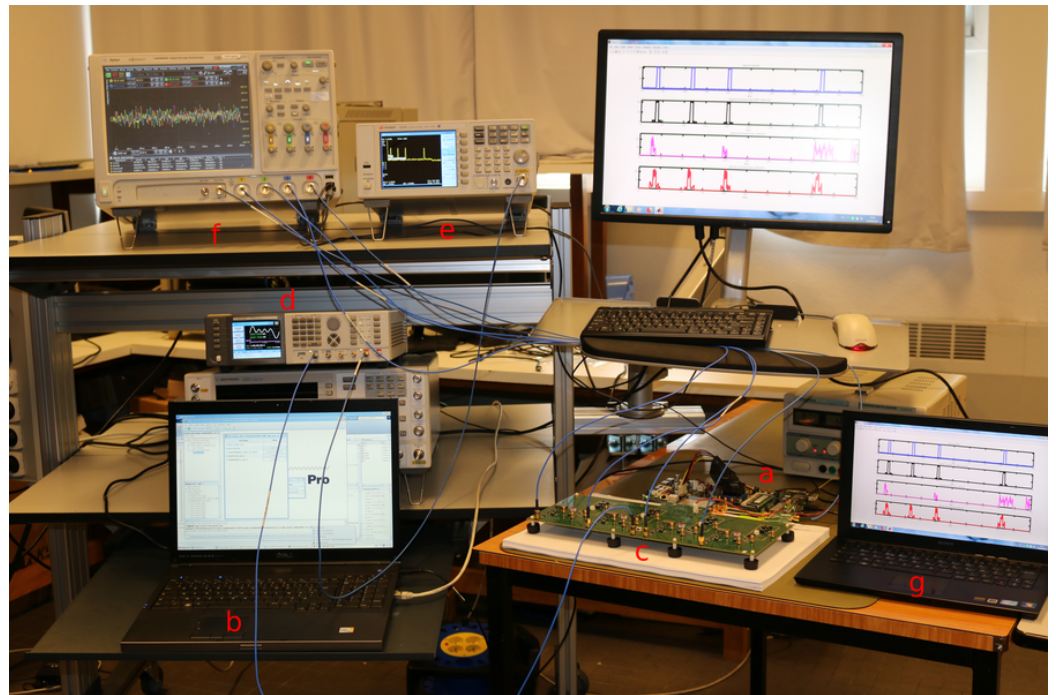


Figure 3. Photo of our compressed sampling testbed: (a) ML605 board for modulating waveform generation, (b) PC control, (c) MWC analog front-end board, (d) Arbitrary waveform generator, (e) Spectrum analyzer, (f) DSO90404A Agilent Infiniium four-channel scope and (g) PC for spectrum reconstruction.

3.1. Prototype Parameters

The Nyquist frequency is set to $F_{Nyq} = 1$ GHz. The number of physical channels is set to $M = 4$ in order to save hardware size and price. Pseudo-random binary signal have been chosen for simplicity of generation for the mixing sequences which length is fixed $L = 96$. In our scenario, the bandwidth of each transmitter is set to $B = 2F_p/3$. To choose the collapsing factor, a trade-off between reasonable total equivalent sampling rate and maximal number of symmetric transmitters $N_{t_{max}}$ must be conducted. Related to the model, the input bandwidth is divided into L subbands with a bandwidth F_p . With this choice, each transmitter can be positioned inside one channel of the MWC or it can be astride at most two channels. The worst case should be taken into account, namely, that each transmitter can locate astride two channels of the equivalent model. We choose a collapsing factor $q = 7$. The condition of sparsity must be verified such as $L_z < M \times q$ where L_z is the maximum number of active channels in the MWC equivalent model. The number of active channels in the MWC equivalent model is strictly set $L_z = M \times q - 1$ and to take into account the worst case that the transmitters can be astride two active channels, then we set $L_{z_{max}} = (M \times q - 1)/2$. Since the transmitters are symmetric in real case; then, we finally set the maximum number of transmitters $N_{t_{max}} = \lfloor L_{z_{max}}/2 \rfloor = \lfloor (M \times q - 1)/4 \rfloor$, which leads to $N_{t_{max}} = 6$. The bandwidth of ideal low-pass filter and ADC (and the sampling rate) is equal to $F_s = qF_{Nyq}/L = 72.9$ MHz, which involves a cut-off frequency $F_c = F_s/2 = 36.5$ MHz. The repetition frequency of modulating waveforms is equal to $F_p = F_{Nyq}/L = 10.4$ MHz. The bandwidth of each transmitter is fixed to $B = 2F_p/3 = 6.9$ MHz. The total equivalent sampling rate is equal to $M \times F_s = 291.6$ MHz which is 29.16 % of the Nyquist rate.

For the rest of the paper, input signal has $N_t = 4$ transmitters which corresponds to the occupancy of 4 subbands which are symmetric, equivalent to occupy $2 \times N_t = 8$ subbands in Nyquist bandwidth.

Table 2 sums up the parameters of the MWC.

Table 2. Parameters of MWC prototype.

Symbol	Meaning	Value
M	Number of MWC channels	4
q	Collapsing factor	7
L	Length of mixing sequence	96
F_{Nyq}	Nyquist frequency	1 GHz
F_p	Repetition rate of mixing sequence	10.4 MHz
F_s	Sampling rate	72.9 MHz
B	Bandwidth of each active subband	6.9 MHz
N_t	Number of transmitters	4
SNR	Signal to Noise Ratio in the transmitting subbands	5, 10, 15, 20, 25, 30, 40 dB

The relation between the Signal to Noise ratio (SNR) in the transmitting subbands and the Signal to Noise ratio in the whole spectrum is computed by:

$$SNR = SNR_{Nyq} + 10 \log_{10} \left(\frac{F_{Nyq}}{2N_t \times B} \right) \quad (6)$$

3.2. Analog Board

A (Avnet) “ML605 DSP Kit with AD/DA board” embedding a (Xilinx) Virtex-6 FPGA is used to generate pseudo-random modulating waveforms. The Gigabit-Transceiver X (GTX) high-speed SERDES (SERializer-DESrializer) transceivers embedded in its (Xilinx) LX240T Virtex-6 FPGA model and the different debugging cores from (Xilinx) Chipscope Pro for the Virtex-6 FPGA gave us the required programmability, speed and development flexibility to output the differential signals implementing the mixing sequences. This allowed us to dynamically choose (per channel) the sequence from a compiled list, fix its size, turn on and off channels, adjust output amplitudes and add some pre-emphasis or post-emphasis effects to signals. With recompilation, we can also add new sequences to the list and change the bit rate. The clock source can be physically changed to appropriate external generators. GTXs 0, 1, 2 and 3 are, respectively, connected to channels 1, 2, 3 and 4 of a MWC analog front-end board.

A Keysight 81180A arbitrary waveform generator is used to generate the input signal. The channel 1 is plugged to a Keysight N9320B spectrum analyzer (range frequency 9 kHz to 3 GHz) to control the simulated input signal and the channel 2 is plugged to a SCA-4-10+ splitter from Mini-Circuits® of the MWC analog front-end board with four channels. Each channel has one M1-0008 mixer from MARki® and one SXLP-36+ low-pass filter from Mini-Circuits® with a cut-off frequency $F_c(-3 \text{ dB}) = 40 \text{ MHz}$. The SXLP-36+ filter has been chosen to match the design of the ideal low-pass filter (sharp cut-off, flat band in frequency range [DC-36] MHz). Figure 4 shows a block diagram of the analog board.

A PC controls the generation of the modulating waveforms with the ML605 board and also the generation of the input signal with the arbitrary waveform generator.

Output signals $y_i(t)$ are acquired and saved by a DSO90404A Agilent Infiniium four-channel scope which provides up 8 GHz real-time bandwidth and 40 Gsample/s sample rate. The outputs are acquired at 40 Gsample/s. To be able to synchronize the acquisition with respect to the modulating waveforms, an extra signal equivalent to a pulse is also generated by the GTX 7 of ML605 board which is plugged to the scope external trigger.

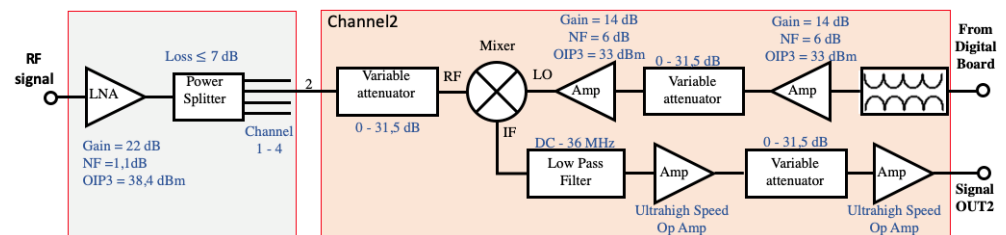


Figure 4. Block diagram of the analog board.

Figure 5 shows our compressed sampling prototype analog front-end board and the ML605 control board.

A PC is used to apply a post-processing for the reconstruction. MWC outputs are downsampled at $F_{SS} = 10 \times F_p = 104$ MHz. Then a digital filter with a bandwidth F_s is applied to eliminate aliasing effect and filtered outputs are downsampled at F_s .

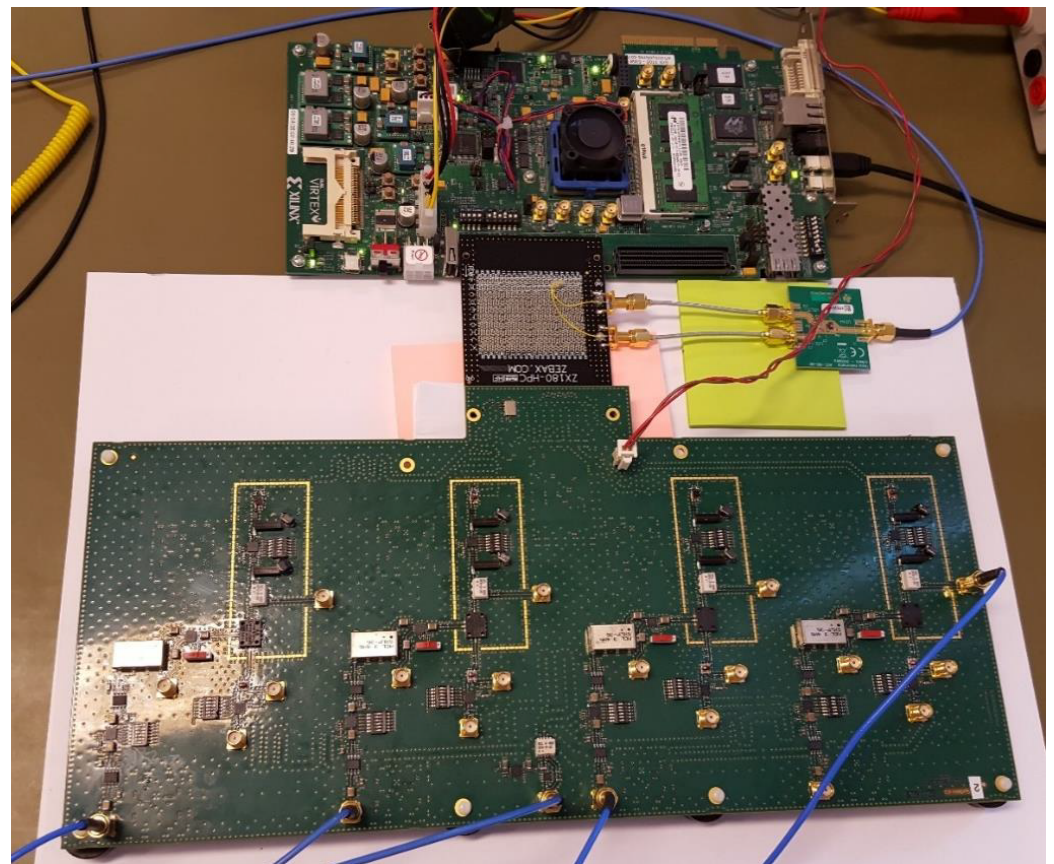


Figure 5. Photo of compressed sampling prototype analog board (bottom) and the ML605 board (top).

3.3. Example of Reconstruction without Calibration

Figure 6 shows an example of spectrum reconstruction without calibration at $SNR = 30$ dB from the theoretical sensing matrix. Each reconstructed spectrum is in linear scale and has been normalized such that the power of each reconstructed spectrum is equal to the power of the input spectrum. Real data have been acquired and saved by the scope. Spectrum reconstruction of measured data with the theoretical sensing matrix (calculated directly from modulating waveforms) have bad detection performances and high false alarm compared to the results obtained for the simulated data. This result is due to incorrect estimation of the sensing matrix linked to analog components. Indeed, analog components introduce phases which change the theoretical sensing matrix. Consequently, the goal of the next section is to present a new calibration method to estimate sensing matrix coefficients.

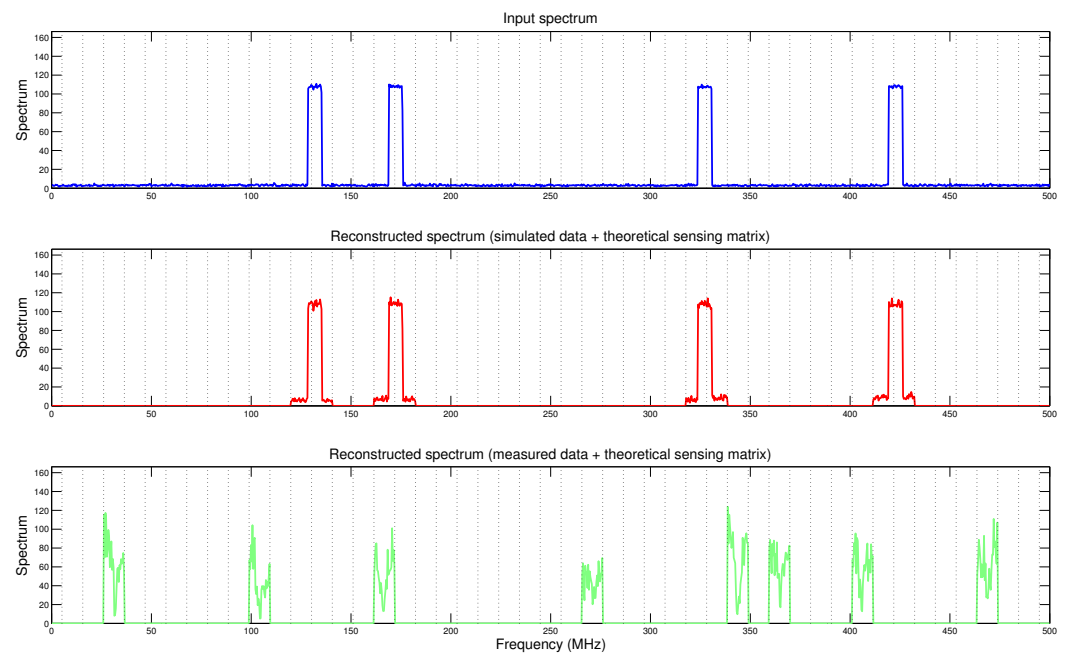


Figure 6. Comparison of reconstructed spectrum with four transmitters and SNR = 30 dB using theoretical sensing matrix (simulated data vs. measured data).

4. Proposed Calibration Method

To ensure correct spectrum recovery, the major problem is to estimate precisely the sensing matrix \mathbf{P}_e . In ideal case, it is possible to compute the sensing matrix by knowing the modulating waveforms. However, in practice, this process brings bad results due to the hardware design such as nonlinearities of mixers and amplifiers, filters deflects, desynchronization of modulating waveforms, connectors and cables. Consequently, a calibration method must be used to estimate sensing matrix coefficients.

In 2014, a calibration method for MWC system, developed by Technion, has been proposed in [23] and provides good reconstruction performance for SNR in the whole spectrum greater than 8 dB. The process estimates the system's response for every frequency band by injecting consecutive sinusoidal inputs at incremental rates. By knowing the sine frequency of input signal and MWC outputs, it is possible to identify one column of the sensing matrix. This step must be repeated with sine functions at different frequencies to estimate all columns of the sensing matrix. From our experience it appears that this process can be long and difficult because the same step must be repeated for all columns. For our system configuration with 96 columns, the process should be repeated 49 times to complete the calibration (due to symmetries, some columns can be estimated by pairs). That is the reason why we propose a new calibration method which estimates the sensing matrix \mathbf{P}_e by injecting a single white noise signal.

Note that the calibration developed by Technion can be considered as a reference. Indeed, researchers who design the MWC system come also from Technion. For the rest of the paper, our results will be compared with those obtained with calibration technique developed by Technion.

4.1. Calibration Algorithm

The calibration algorithm is divided into two main steps: preprocessing resynchronization step and sensing matrix estimation step.

A specific white noise signal, called "calibration signal", is first generated (Figure 7). This signal is periodic with the period equal to the size of the block used for the reconstruction. Its basic pattern (N samples at F_{nyq}) is first generated in the Fourier domain, specifying perfectly flat amplitudes and random phases, then an inverse-Fast Fourier Transform (FFT) provides the samples in the time domain.

After injection of input signal, the outputs of MWC system are recorded. In parallel, we also record a pulse wave (output of GTX 7) which identifies the beginning of modulating waveforms.

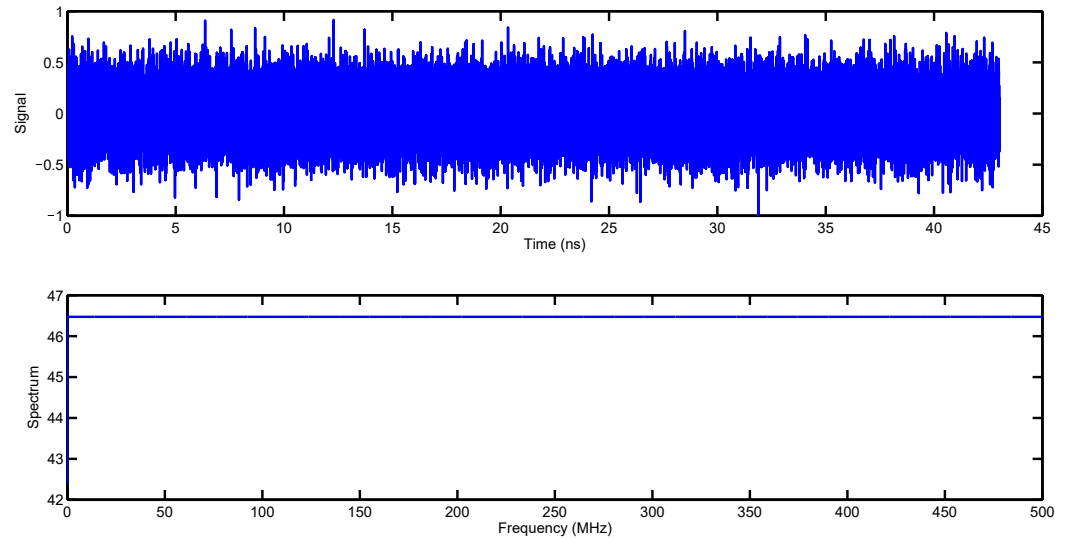


Figure 7. Representation of calibration signal in time and frequency domains.

4.1.1. Resynchronization Preprocessing Step

The resynchronization preprocessing step estimates the optimal shift value d_{opt} which minimizes the Frobenius norm (or maximizes the inverse Frobenius norm) of the residual matrix between shifted version of output signal and reconstructed output (relative to the equivalent model) knowing the input signal.

To complete the calibration, we must synchronize three signals:

- the input calibration signal (composed of a repetition of N samples blocks);
- the modulating waveforms;
- the MWC outputs.

In practice, it is possible to synchronize together only two signals (for example, the outputs and the pulse wave which identifies the modulating waveforms starts), but not three signals. To achieve this task, digital processing must be followed.

Figure 8 illustrates the synchronization method. At the beginning of the process, we know:

- The synchronization pulse wave (output of GTX 7) related to the modulating waveforms;
- The periodic pattern of the input signal with no knowledge of the delay;
- The four outputs of MWC.

Firstly, a coarse synchronization is conducted to determine the starting sample value d_{coarse} corresponding of the beginning of the input pattern. Let us note $N_s = NF_s / F_{nyq}$ the number of samples in an output block (corresponding to an input block of N samples). Output blocks, shifted by $d \in [0; 2N_s - 1]$ samples from the beginning of recorded output \mathbf{y}_p , noted \mathbf{y}_{p_d} , are formed to be able to estimate d_{coarse} . By knowing \mathbf{z}_c , which is the vector \mathbf{z} restricted to its active components, with Equation (3), and using the pseudo-inverse with Equation (4), the sensing matrix $\hat{\mathbf{P}}_e$ can be estimated by:

$$\hat{\mathbf{P}}_e = \mathbf{y}_{p_d} \mathbf{z}_c^* (\mathbf{z}_c \mathbf{z}_c^*)^{-1} \tag{7}$$

Then, the reconstructed signal \mathbf{y}_{r_d} relative to the equivalent model knowing the input signal is computed by:

$$\mathbf{y}_{r_d} = \hat{\mathbf{P}}_e \mathbf{z}_c = \mathbf{y}_{p_d} \mathbf{z}_c^* (\mathbf{z}_c \mathbf{z}_c^*)^{-1} \mathbf{z}_c \tag{8}$$

d_{coarse} is obtained by minimizing the Frobenius norm on the residual matrix $\mathbf{R} = \mathbf{y}_{r_d} - \mathbf{y}_{p_d}$:

$$d_{coarse} = \min_{d \in [0; N_s - 1]} \|\mathbf{y}_{r_d} - \mathbf{y}_{p_d}\|_F \tag{9}$$

with $\|\cdot\|_F$ the Frobenius norm.

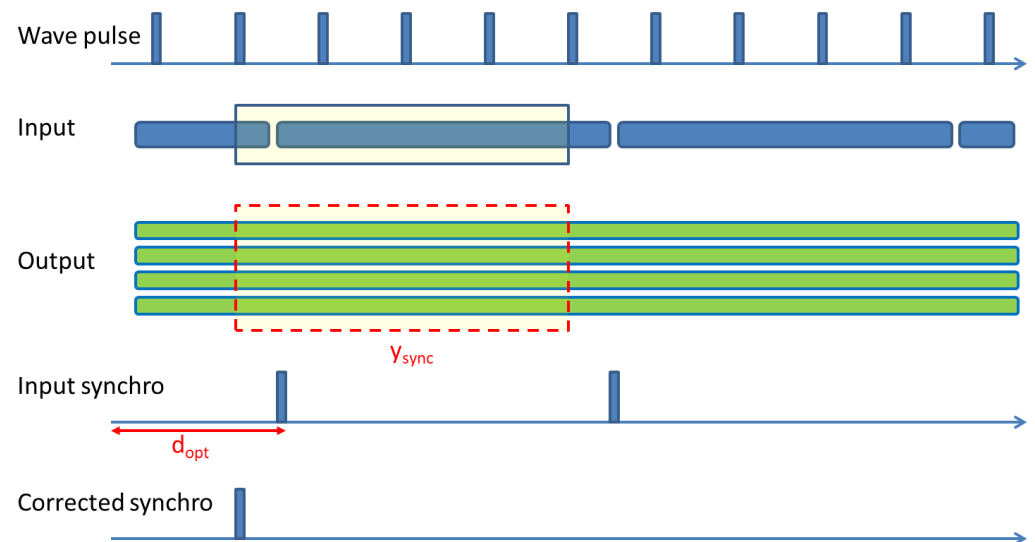


Figure 8. Synchronization between input signal, modulating waveforms and MWC outputs.

For example, d_{coarse} is equal to 2041 in Figure 9. Note that for easier visualization it is the inverse of the Frobenius norm (with respect to d) which is shown on the figure.

Since, as previously mentioned, we computed it for $d \in [0; 2N_s - 1]$, we have two peaks on Figure 9, while computation could be restricted to $d \in [0; N_s - 1]$, this extension is preferred, in order to confirm visually (by the presence of two similar peaks separated by N_s samples) the validity of the obtained synchronization.

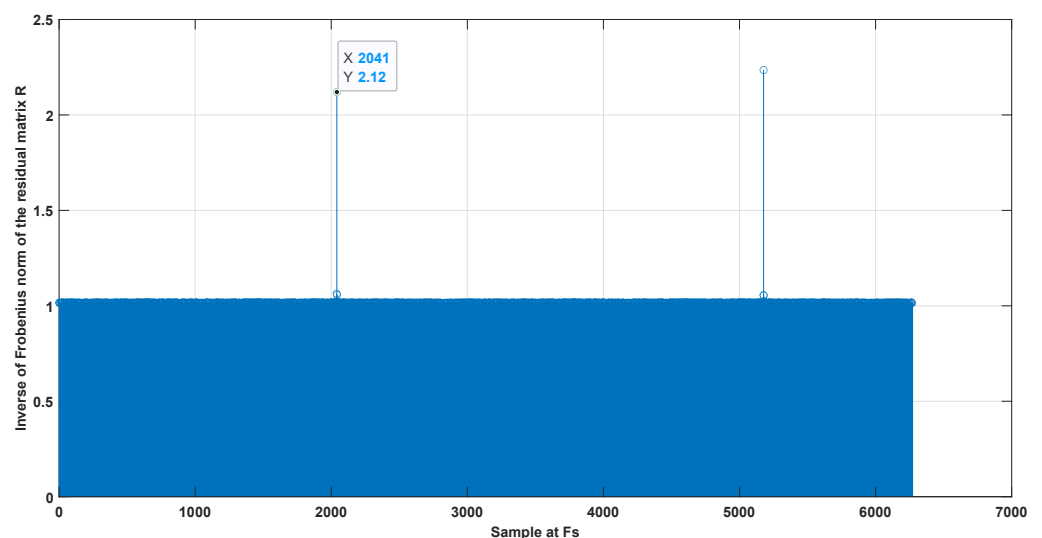


Figure 9. Coarse synchronization with identification of pulses.

A fine synchronization (see Figure 10) is then performed. Small corrections $d_{fine} \in [-2; 2]/32$ are applied to d_{coarse} and evaluated using the same procedure as described above, that is using Equation (7), Equation (8) and Equation (9). The samples required for this fine synchronization are obtained by oversampling the outputs by a factor 32. The computational load remains small because we have to test only a few values of d_{fine} .

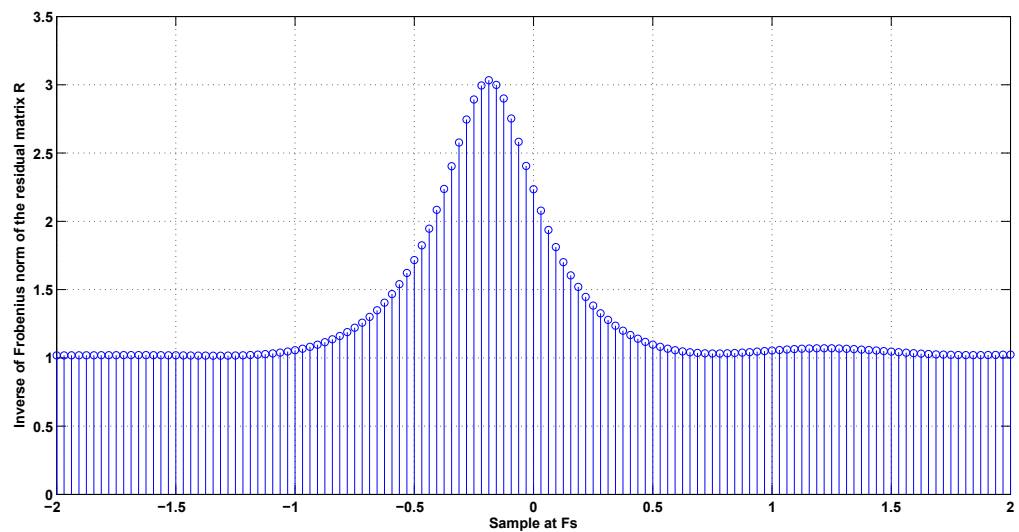


Figure 10. Fine synchronization.

Now, we know that the first output block corresponding to an input pattern starts at $d_{opt} = d_{coarse} + d_{fine}$ samples from the beginning. This is represented by “input synchro” in Figure 8.

However, at this step, the calibration can not be conducted because there is no reason that the “input synchro” is synchronous with the modulating waveforms. To solve this problem, the second step enables to select the time corresponding to the pulse of modulating waveform which has just preceded the “input syncho”. We obtained a corrected synchronization (“corrected synchro” in Figure 8), which is now synchronous with the modulating waveforms, but not with the input pattern anymore. To solve this problem, we recalculated the input pattern (framed part in Figure 8). This was easy to carry out because we know that the input signal is periodic, so it is just a circular permutation of the input pattern.

4.1.2. Sensing Matrix Estimation Step

By knowing the corrected input pattern and the synchronized outputs of MWC system y_{sync} , it is possible to estimate the sensing matrix with only one step. The estimated sensing matrix \hat{P}_e is equal to:

$$\hat{P}_e = y_{sync} z_c^* (z_c z_c^*)^{-1} \tag{10}$$

Note that the z_c which appears in this equation has been recomputed because it now corresponds to the corrected input pattern.

4.2. Examples of Calibration Sensing Matrices

To validate the programming of the reference calibration method, the sensing matrix coefficients are firstly estimated by using Matlab simulation. Figure 11a shows the modulus of the theoretical sensing matrix P_e and estimated sensing matrix obtained by the reference calibration method $\hat{P}_{e,ref}$. The modulus of the difference between the theoretical and estimated sensing matrices shows that the matrices are equal because the maximum of the difference is very small, i.e., less than 12×10^{-8} . The same conclusion can be conducted with the sensing matrix $\hat{P}_{e,our\ method}$ estimated by our method (Figure 11b). However, our proposed calibration method seems to be more accurate because the maximum of modulus of the difference between the theoretical and estimated sensing matrices is less than 2.5×10^{-15} .

Figure 12 shows the comparison between theoretical matrix and calibration matrices estimated from real measurements. The estimated sensing matrices have been normalized relative to the Frobenius norm of the theoretical sensing matrix.

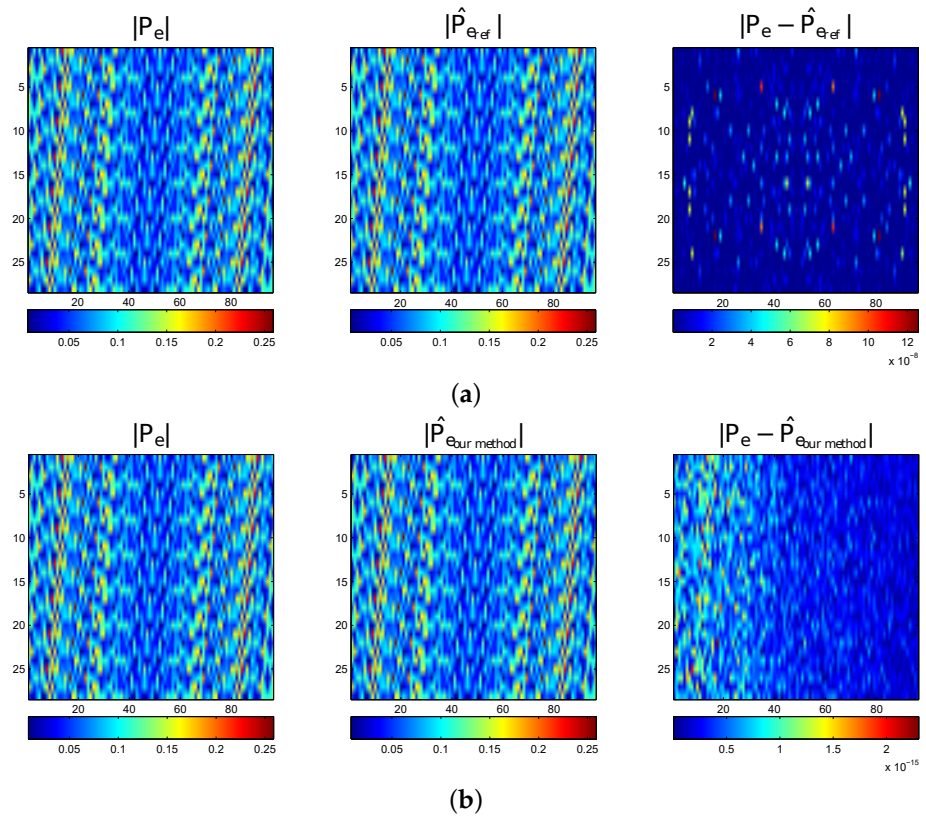


Figure 11. Comparison between theoretical matrix and calibration matrices with Matlab simulation (**left:** Modulus of theoretical sensing matrix; **middle:** Modulus of estimated sensing matrix; **right:** Modulus of difference). (a) Reference calibration. (b) Our proposed calibration.

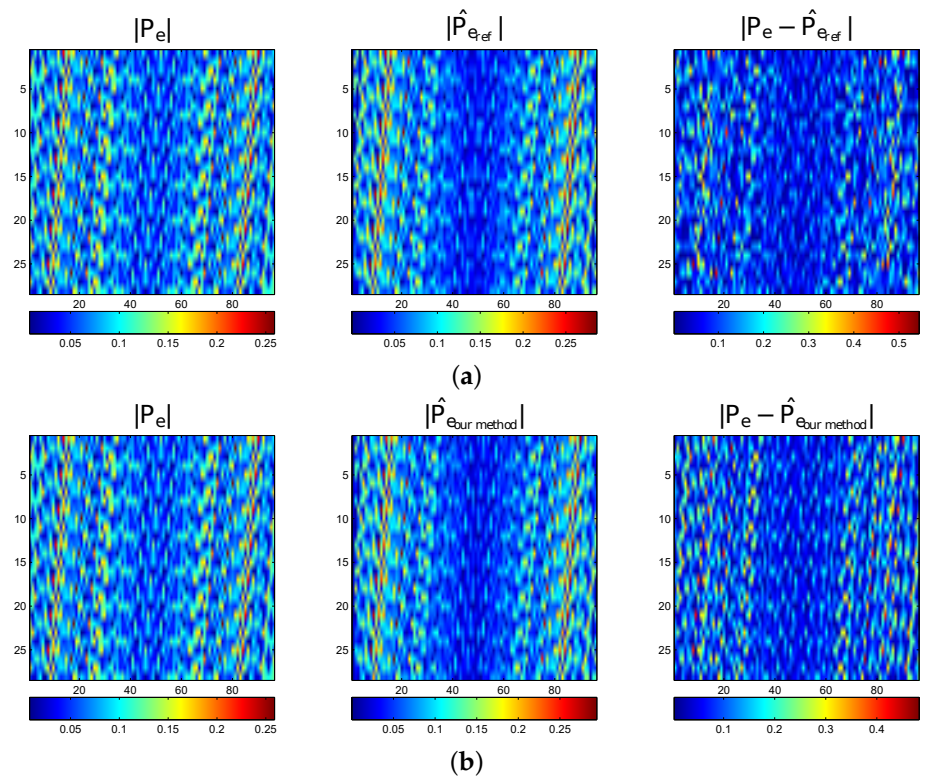


Figure 12. Comparison between theoretical matrix and calibration matrices estimated from real measurements (**left:** Modulus of theoretical sensing matrix; **middle:** Modulus of estimated sensing matrix; **right:** Modulus of difference). (a) Reference calibration. (b) Our proposed calibration.

Although these matrices have strong similarities, the modulus of the difference between the theoretical and estimated sensing matrices shows that the matrices are quite different. That is the reason why the calibration is essential.

The next section presents reconstruction performances of our proposed calibration method compared to the reference calibration method.

5. Performances

In order to prove the efficiency of the proposed calibration method, the probabilities of correct reconstruction and false alarm are measured and studied correspondingly to the levels of SNR. The results are compared to those obtained with the theoretical MWC scheme and data from the prototype without calibration and with the reference calibration method [23].

Based on the principle of the MWC, the input bandwidth is divided into L subbands with a bandwidth F_p (dash lines in Figure 13 represent subbands for positive frequencies). The goal of reconstruction algorithm is to seek the active subbands, which contain the information of input signal. Denote B_d the detected subband from the MWC output and B_r the real subband from input signal.

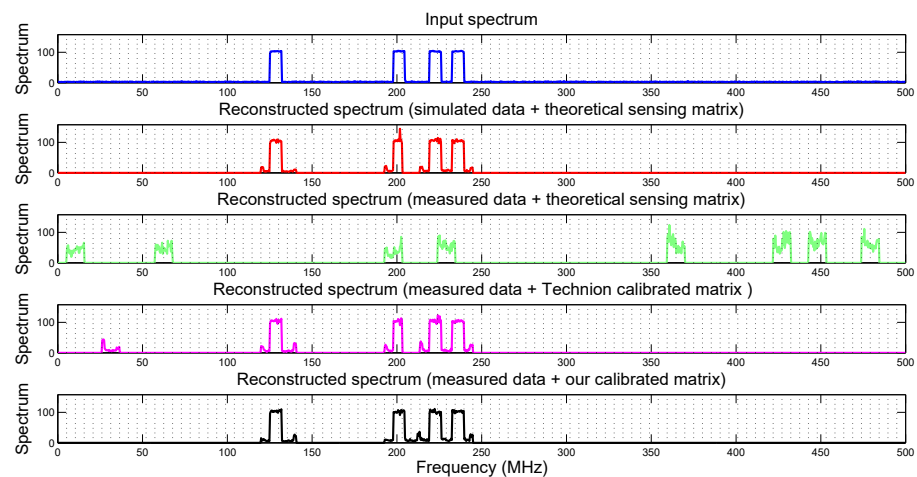


Figure 13. Comparison of reconstructed spectrum (4 transmitters, SNR = 30 dB).

The probability of correct detection P_c includes the expected activity elements among all the reconstructed activity elements in the reconstructed channel; and P_c is estimated by the percentage of occupation between the detected and real channels related to the real channels occupied by the spectrum:

$$P_c = \frac{\%(B_r \cap B_d)}{\%B_r}, \tag{11}$$

where B_d is the detected channels occupation and B_r is the real channels occupation.

The probability of false alarm P_{fa} is the unexpected subbands which are introduced by the MWC output. The probability P_{fa} is determined by the percentage of detected subbands different to real subbands occupation which intersect the complement of real subbands occupied by the spectrum:

$$P_{fa} = \frac{\%(B_d \setminus B_r) \cap \bar{B}_r}{1 - \%B_r}. \tag{12}$$

Correct reconstruction and false alarm rates are averaged over 50 trials for each SNR belonging to 5, 10, 15, 20, 25, 30 and 40 dB. Central frequencies of each subband of the test signals have been randomly generated.

Figure 13 illustrates an example of spectrum reconstruction (4 transmitters at SNR = 30 dB) obtained with theoretical MWC scheme and data from prototype with calibration versus

without calibration. It can be noted that the locations of input spectrum are correctly reconstructed with the calibration and similar to the theoretical MWC scheme whereas the results are bad in location and high false alarm without calibration. Compared to the theoretical MWC scheme, more noise is reconstructed with the calibration due to the additional noise of analog components. Note that one false alarm appears for the frequency range [26;36.5] MHz with the reference method. Figure 14a (resp. Figure 14b) is obtained by zooming Figure 13 between frequency range [119;136] MHz (resp. [190;209] MHz) and by plotting the input spectrum and spectrum reconstructed with the reference calibrated matrix and with our calibrated matrix. From Figure 14a, it is clear that the position of the transmitter has been correctly detected by both calibration methods. In the transmitter subband, amplitudes reconstructed with both calibration methods are slightly different due to the effect of noise. In the active subbands, the only noise is reconstructed depending on the calibration method. Figure 14b illustrates partial reconstruction of transmitter position obtained with the reference method whereas our calibration method can correctly detect transmitter position.

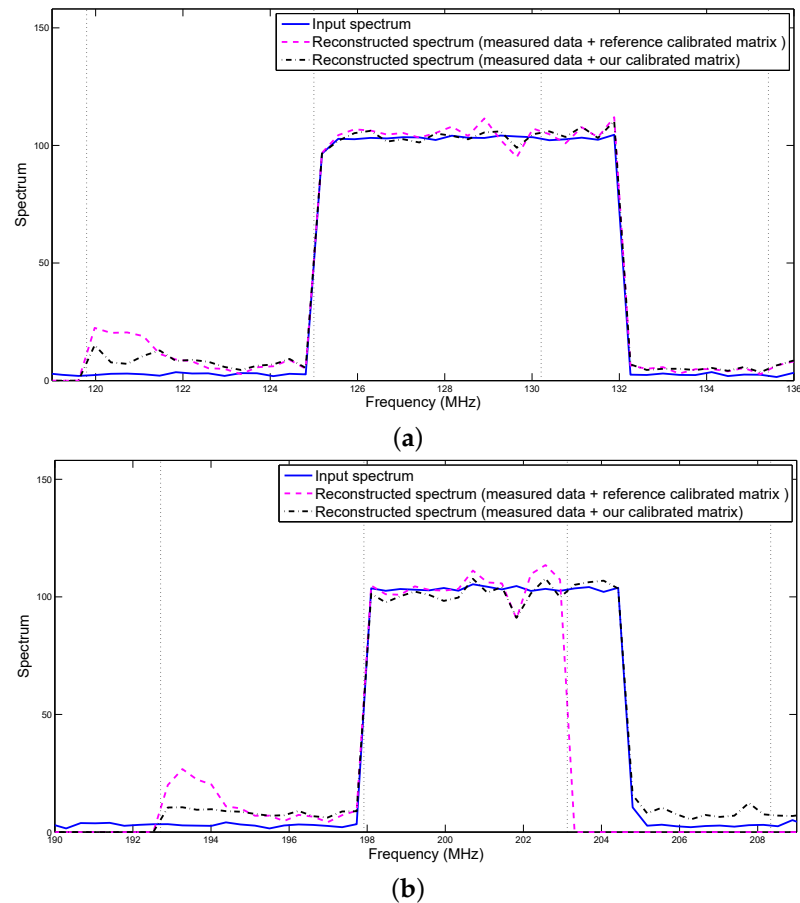
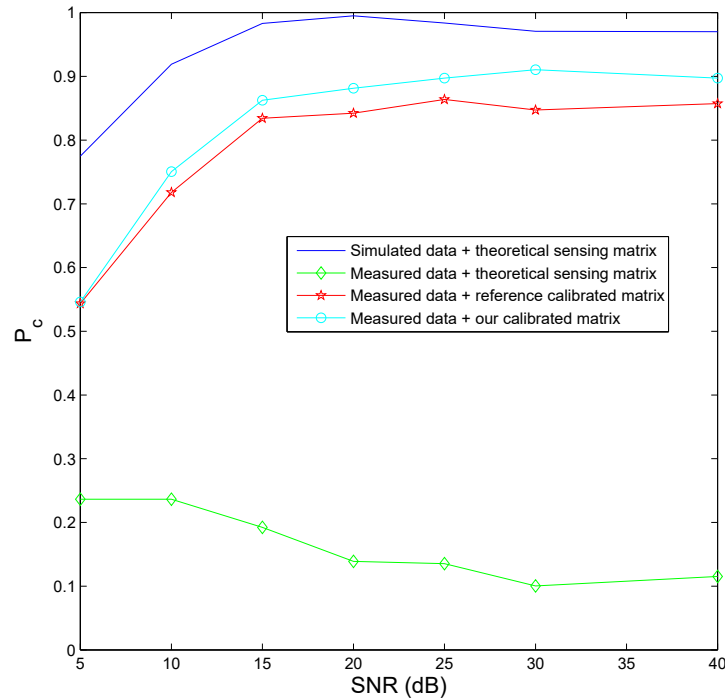


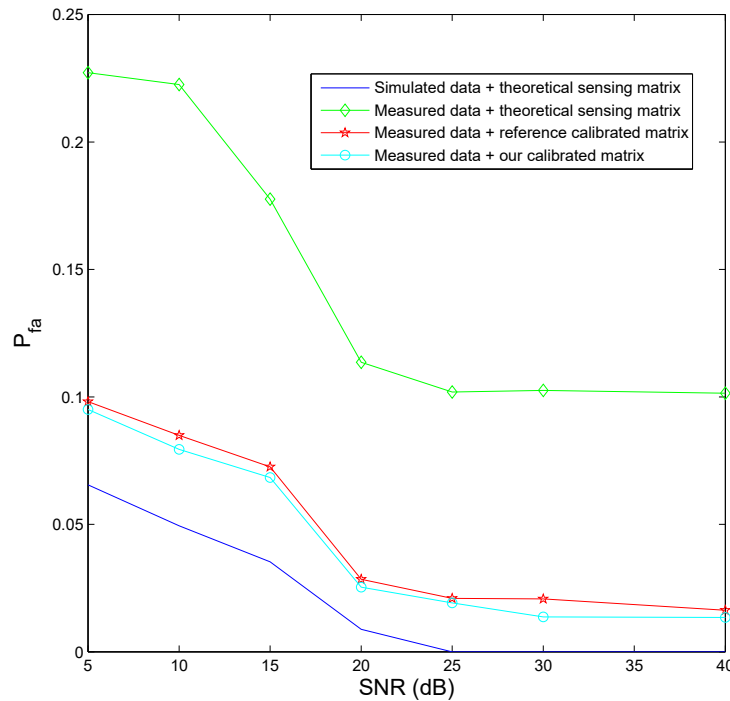
Figure 14. Zoom of Figure 13 between frequency ranges [119;136] MHz and [190;209] MHz. (a) Example of correct reconstruction of transmitter position obtained with both calibration methods. (b) Example of partial (resp. correct) reconstruction of transmitter position obtained with the reference method (resp. our method).

Figure 15 presents correct reconstruction and false alarm rates at each SNR level. It can be seen that the proposed calibration method provides high performance above 15 dB SNR, which is approximately equal to 2.4 dB in the whole spectrum. Our proposed method seems to give slightly better results compared to the reference calibration method. Indeed, correct reconstruction rates are 6 % higher than the reference calibration method and false alarm rates are lower for low SNRs. The results obtained without calibration show that

it is essential to complete a calibration because the correct reconstruction rates are very low and the false alarm rates are very high. We also show the results obtained with the theoretical MWC in simulation. The correct reconstruction are greater than those obtained with the calibration. The difference can be explained by the impact of measurement on the reconstruction. For low SNR, we obtained high correct reconstruction and false alarm rates because there is an overestimation of the number of active channels.



(a)



(b)

Figure 15. Correct reconstruction and false alarm rates in function of SNRs. (a) Correct reconstruction rate. (b) False alarm rate.

6. Conclusions

This paper presents a new hardware calibration method of Modulated Wideband Converter based on a single measurement of a white noise signal with advanced resynchronization preprocessing. The proposed method has the advantage to be simple and time saving compared to methods based on iterative single-tones or mixture of single-tones signals. The proposed method has been used to estimate the calibrated sensing matrix coefficients from our prototype of Compressed Sampling based on Modulated Wideband Converter scheme. Calibration performances have been evaluated with percent of correct reconstruction and false alarm averaged over 50 trials for 7 SNRs. As expected, the spectrum reconstruction from measured data fails with the theoretical sensing matrix. The proposed method proves that reconstruction with calibrated matrix provides high performance for SNRs in the whole spectrum higher than 2.4 dB compared to the reference calibration method.

Author Contributions: Conceptualization, G.B.; methodology, G.B., A.F., R.G. and A.M.-G.; software, G.B., A.F. and R.G.; validation, G.B., A.F. and R.G.; formal analysis, G.B., A.F. and R.G.; investigation, G.B., A.F. and R.G.; resources, G.B., A.F. and R.G.; data curation, G.B., A.F., R.G. and A.M.-G.; writing—original draft preparation, G.B., A.F. and R.G.; writing—review and editing, G.B., A.F. and R.G.; visualization, G.B., A.F. and R.G.; supervision, R.G.; project administration, A.F. and R.G.; funding acquisition, G.B. and R.G. All authors have read and agreed to the published version of the manuscript.

Funding: This research is partly supported by the RAPID REACC-RF project and by the IBNM (Brest Institute of Computer Science and Mathematics) CyberIoT Chair of Excellence at the University of Brest, and the Brittany region—Pôle d'Excellence Cyber.

Data Availability Statement: The data presented in this study are available on request from the corresponding author.

Acknowledgments: The authors would like to thank the company Syrlinks for the design of the analog board.

Conflicts of Interest: The authors declare no conflict of interest.

Abbreviations

The following abbreviations are used in this manuscript:

MWC	Modulated Wideband Converter
CS	Compressed Sensing
IoT	Internet of Things
ADC	Analog to Digital Converter
IDFT	Inverse Discrete Fourier Transform
CFT	Continuous-To-Finite
OMP	Orthogonal Matching Pursuit
SNR	Signal to Noise Ratio
GTX	Gigabit-Transceiver X
SERDES	SERializer-DESrializer
FFT	Fast Fourier Transform

References

1. Shannon, C.E. Communication in the presence of noise. *Proc. IRE* **1949**, *37*, 10–21. [[CrossRef](#)]
2. Nyquist, H. Certain topics in telegraph transmission theory. *Trans. Am. Inst. Electr. Eng.* **1928**, *47*, 617–644. [[CrossRef](#)]
3. Kester, W. (Ed.) *Data Conversion Handbook*; Newnes: Oxford, UK, 2005; p. 76.
4. Laska, J.N.; Kirolos, S.; Duarte, M.F.; Ragheb, T.S.; Baraniuk, R.G.; Massoud, Y. Theory and implementation of an analog-to-information converter using random demodulation. In Proceedings of the IEEE International Symposium on Circuits and Systems, New Orleans, LA, USA, 27–30 May 2007; pp. 1959–1962.
5. Tropp, J.A.; Laska, J.N.; Duarte, M.F.; Romberg, J.K.; Baraniuk, R.G. Beyond Nyquist: Efficient sampling of sparse bandlimited signals. *IEEE Trans. Inf. Theory* **2010**, *56*, 520–544. [[CrossRef](#)]

6. Venkataramani, R.; Bresler, Y. Perfect reconstruction formulas and bounds on aliasing error in sub-Nyquist nonuniform sampling of multiband signals. *IEEE Trans. Inf. Theory* **2000**, *46*, 2173–2183. [[CrossRef](#)]
7. Yang, L.; Fang, J.; Duan, H.; Li, H. Fast compressed power spectrum estimation: toward a practical solution for wideband spectrum sensing. *IEEE Trans. Wirel. Commun.* **2019**, *19*, 520–532. [[CrossRef](#)]
8. Mishali, M.; Eldar, Y.C. From theory to practice: Sub-Nyquist sampling of sparse wideband analog signals. *IEEE J. Sel. Top. Signal Process.* **2010**, *4*, 375–391. [[CrossRef](#)]
9. Yazicigil, R.T.; Haque, T.; Whalen, M.R.; Yuan, J.; Wright, J.; Kinget, P.R. Wideband rapid interferer detector exploiting compressed sampling with a quadrature analog-to-information converter. *IEEE J. Solid-State Circuits* **2015**, *50*, 3047–3064. [[CrossRef](#)]
10. Yazicigil, R.T.; Haque, T.; Kumar, M.; Yuan, J.; Wright, J.; Kinget, P.R. A compressed-sampling time-segmented quadrature analog-to-information converter for wideband rapid detection of up to 6 interferers with adaptive thresholding. In Proceedings of the 2016 IEEE Radio Frequency Integrated Circuits Symposium (RFIC), San Francisco, CA, USA, 22–24 May 2016; pp. 282–285.
11. Zhao, Y.; Hu, Y.H.; Liu, J. Random triggering-based sub-Nyquist sampling system for sparse multiband signal. *IEEE Trans. Instrum. Meas.* **2017**, *66*, 1789–1797. [[CrossRef](#)]
12. Pelissier, M.; Studer, C. Non-uniform wavelet sampling for RF analog-to-information conversion. *IEEE Trans. Circuits Syst. I Regul. Pap.* **2017**, *65*, 471–484. [[CrossRef](#)]
13. De Vito, L.; Iadarola, G.; Lamonaca, F.; Picariello, F.; Rapuano, S.; Tudosa, I. Non-uniform wavelet bandpass sampling analog-to-information converter: A hardware implementation and its experimental assessment. *Measurement* **2019**, *134*, 739–749. [[CrossRef](#)]
14. Landau, H.J. Necessary density conditions for sampling and interpolation of certain entire functions. *Acta Math.* **1967**, *117*, 37–52. [[CrossRef](#)]
15. Papoulis, A. Generalized sampling expansion. *IEEE Trans. Circuits Syst.* **1977**, *24*, 652–654. [[CrossRef](#)]
16. Lin, Y.P.; Vaidyanathan, P. Periodically nonuniform sampling of bandpass signals. *IEEE Trans. Circuits Syst. II Analog. Digit. Signal Process.* **1998**, *45*, 340–351.
17. Upadhyaya, V.; Salim, M. Compressive Sensing: Methods, Techniques, and Applications. In Proceedings of the IOP Conference Series: Materials Science and Engineering, Jeju Island, Korea, 12–14 March 2021; IOP Publishing: Bristol, UK, 2021; Volume 1099, p. 012012.
18. Fang, J.; Wang, B.; Li, H.; Liang, Y.C. Recent Advances on Sub-Nyquist Sampling-Based Wideband Spectrum Sensing. *IEEE Wirel. Commun.* **2021**, *28*, 115–121. [[CrossRef](#)]
19. Candès, E.J.; Wakin, M.B. An introduction to compressive sampling. *IEEE Signal Process. Mag.* **2008**, *25*, 21–30. [[CrossRef](#)]
20. Donoho, D.L. Compressed sensing. *IEEE Trans. Inf. Theory* **2006**, *52*, 1289–1306. [[CrossRef](#)]
21. Zelnik-Manor, L.; Rosenblum, K.; Eldar, Y.C. Sensing matrix optimization for block-sparse decoding. *IEEE Trans. Signal Process.* **2011**, *59*, 4300–4312. [[CrossRef](#)]
22. Abolghasemi, V.; Ferdowsi, S.; Makkiabadi, B.; Sanaei, S. On optimization of the measurement matrix for compressive sensing. In Proceedings of the European Signal Processing Conference, Aalborg, Denmark, 23–27 August 2010.
23. Israeli, E.; Tsiper, S.; Cohen, D.; Shoshan, E.; Hilgendorf, R.; Reysenson, A.; Eldar, Y.C. Hardware calibration of the modulated wideband converter. In Proceedings of the Global Communications Conference (GLOBECOM), Austin, TX, USA, 8–12 December 2014; pp. 948–953.
24. Adams, D.; Eldar, Y.C.; Murmann, B. A Mixer Front End for a Four-Channel Modulated Wideband Converter With 62-dB Blocker Rejection. *IEEE J. Solid-State Circuits* **2017**, *52*, 1286–1294. [[CrossRef](#)]
25. Mishali, M.; Eldar, Y.C.; Dounaevsky, O.; Shoshan, E. Sub-Nyquist acquisition hardware for wideband communication. In Proceedings of the 2010 IEEE Workshop on Signal Processing Systems, San Francisco, CA, USA, 6–8 October 2010; pp. 156–161.
26. Mishali, M.; Eldar, Y.C.; Dounaevsky, O.; Shoshan, E. Xampling: Analog to digital at sub-Nyquist rates. *IET Circuits Devices Syst.* **2011**, *5*, 8–20. [[CrossRef](#)]
27. Eldar, Y.C. *Sampling Theory: Beyond Bandlimited Systems*; Cambridge University Press: Cambridge, UK, 2015.
28. Cohen, D.; Tsiper, S.; Eldar, Y.C. Analog-to-Digital Cognitive Radio: Sampling, Detection, and Hardware. *IEEE Signal Process. Mag.* **2018**, *35*, 137–166. [[CrossRef](#)]
29. Liu, W.; Huang, Z.; Wang, X.; Sun, W. Design of a single channel modulated wideband converter for wideband spectrum sensing: Theory, architecture and hardware implementation. *Sensors* **2017**, *17*, 1035. [[CrossRef](#)] [[PubMed](#)]
30. Wang, P.; You, F.; He, S. An improved signal reconstruction of modulated wideband converter using a sensing matrix built upon synchronized modulated signals. *Circuits Syst. Signal Process.* **2019**, *38*, 3187–3210. [[CrossRef](#)]
31. Fu, N.; Jiang, S.; Deng, L.; Qiao, L. Successive-phase correction calibration method for modulated wideband converter system. *IET Signal Process.* **2019**, *13*, 624–632. [[CrossRef](#)]
32. Park, J.; Jang, J.; Lee, H.N. A calibration for the modulated wideband converter using sinusoids with unknown phases. In Proceedings of the 2017 Ninth International Conference on Ubiquitous and Future Networks (ICUFN), Milan, Italy, 4–7 July 2017; pp. 951–955.
33. Alp, Y.K.; Korucu, A.B.; Karabacak, A.T.; Gürbüz, A.C.; Arıkan, O. Online calibration of modulated wideband converter. In Proceedings of the 2016 24th Signal Processing and Communication Application Conference (SIU), Zonguldak, Turkey, 16–19 May 2016; pp. 913–916.

34. Byambadorj, Z.; Asami, K.; Yamaguchi, T.; Higo, A.; Fujita, M.; Iizuka, T. A Calibration Technique for Simultaneous Estimation of Actual Sensing Matrix Coefficients on Modulated Wideband Converters. *IEEE Trans. Circuits Syst. I Regul. Pap.* **2020**, *67*, 5561–5573. [[CrossRef](#)]
35. Byambadorj, Z.; Asami, K.; Yamaguchi, T.J.; Higo, A.; Fujita, M.; Iizuka, T. High-Precision Sub-Nyquist Sampling System Based on Modulated Wideband Converter for Communication Device Testing. *IEEE Trans. Circuits Syst. I Regul. Pap.* **2021**, *69*, 378–388. [[CrossRef](#)]
36. Mishali, M.; Hilgendorf, R.; Shoshan, E.; Rivkin, I.; Eldar, Y.C. Generic sensing hardware and real-time reconstruction for structured analog signals. In Proceedings of the 2011 IEEE International Symposium of Circuits and Systems (ISCAS), Rio de Janeiro, Brazil, 15–18 May 2011; pp. 1748–1751.
37. Akaike, H. A new look at the statistical model identification. *IEEE Trans. Autom. Control* **1974**, *19*, 716–723. [[CrossRef](#)]
38. Rissanen, J. A universal prior for integers and estimation by minimum description length. *Ann. Stat.* **1983**, *11*, 416–431. [[CrossRef](#)]
39. Cai, T.T.; Wang, L. Orthogonal matching pursuit for sparse signal recovery with noise. *IEEE Trans. Inf. Theory* **2011**, *57*, 4680–4688. [[CrossRef](#)]